

## Regenerated Cellulose from Oil Palm Empty Fruit Bunch using Ionic Liquids Mixture

Noor Syafiqah Hassin<sup>1,2\*</sup>, Izan Izwan Misnon<sup>1,2\*</sup>, Rasidi Roslan<sup>1,2</sup>, Mohd Rozi Ahmad<sup>3</sup>, Latifah Jasmani<sup>4</sup> and Rajan Jose<sup>1,2</sup>

<sup>1</sup>Center for Advanced Intelligent Materials, Universiti Malaysia Pahang, 26300 Pahang, Malaysia.

<sup>2</sup>Faculty of Industrial Sciences and Technology, Universiti Malaysia Pahang, 26300 Pahang, Malaysia.

<sup>3</sup>Textile Research Group, Faculty of Applied Sciences Universiti Teknologi MARA, 40450 Shah Alam, Selangor, Malaysia

<sup>4</sup>Pulp and Paper Laboratory, Forest Products Division, Forest Research Institute Malaysia (FRIM), 52109 Kepong, Selangor, Malaysia

**ABSTRACT** – This work focused on the synthesis of regenerated cellulose (RC) using ionic liquids (ILs) mixture of 1-Ethyl-3-methylimidazolium acetate (EMIMAc) and 1-Ethyl-3-methylimidazolium chloride (EMIMCl) with oil palm empty fruit bunch (OPEFB) cellulose pulp. The IL-OPEFB mixture were prepared at temperature of 100 °C and stirring speed of 270 rpm; subsequently undergoes dry-jet wet spinning using self-designed water coagulation bath. The morphology, structural, and mechanical properties of regenerated cellulose filament (RCF) were characterized by scanning electron microscope (SEM), optical microscopy, Fourier-transform infrared spectroscopy (FTIR), thermal gravimetric analysis (TGA) and tensile machine. An Icell-type RCF was obtained showing good mechanical properties with a tensile strength of  $160.45 \pm 0.699$  MPa, a tenacity of  $8.774 \pm 0.699$  cN/tex, Young's modulus of  $83.245 \pm 1.183$  MPa and 12.92% elongation at break. The RCF had a smooth surface with a round, rigid and hard to break structure are foreseen to have wide applications in sustainable material technology.

### ARTICLE HISTORY

Received: 11<sup>th</sup> Mar 2022

Revised: 27<sup>th</sup> July 2022

Accepted: 09<sup>th</sup> Dec 2022

### KEYWORDS

*Biomass*

*Sustainable Technology*

*Dry-jet Wet Spinning*

*Thermal Stability*

*Cellulose*

## INTRODUCTION

Cellulose has wide application in fiber, film, paper, polymer, and food industries. This is due to its excellent properties; biocompatibility, renewability, non-toxic, hydrophilic, thermal & chemically stability, and it has a limitless source in nature [1–4]. Although cellulose can be extracted from most bio-based precursors such as corn, sugar cane, and wheat, there is competition with food industries as it is edible derivatives. Malaysia is the second-largest oil palm producer and until 2021, 19.6 million tonnes of crude palm oil has been produced [5, 6]. Palm oil industries produce approximately 50% of biomass residue, and 23% are EFB [7] with 62.9% cellulose content [8]. Hence, this work attempts to select OPEFB cellulose from a non-edible source, abundant and relatively cheap.

Cellulose is insoluble in water and the most common organic solvent. Ionic liquids (ILs) as cellulose solvent was firstly reported in 2002 by disrupting the intermolecular hydrogen-bonding network in cellulose [9]. The notable properties of ILs include low melting point, high thermal stability, and high conductivity [2, 10, 11]. There are possibilities to alter and enhance the efficiency of ILs according to a specific application by the independent selection of constituting cation and anion. In this work, the dissolution of cellulose is by using two mixture of ILs with similar cation, which is EMIMAc and EMIMCl. This ILs selection is targeting that the low ILs viscosity resulted in the avoidance of crystallization peak of excess salt from EMIMCl [12, 13]. Furthermore, a previous study of cellulose dissolution claimed that acetate, chloride, and formate were the most promising anion groups [14].

The dry-jet wet spinning method in the filament process consists of the elongational melt polymer flowing in the air gap region and regenerating in a water coagulation bath [15]. This technology is able to produce high-quality properties of RCF [10, 16–18]. Furthermore, the air gap between the spinneret and water, draw ratio, and water bath temperature significantly affects the properties of RCF [19]. In this article, only the suitability of OPEFB in ILs dissolution and RCF properties is presented.

## MATERIALS AND METHOD

The OPEFB cellulose pulp with a degree of polymerization (DP) value of 673 were supplied from Forest Research Institute Malaysia (FRIM) and dried overnight in an oven at 60 °C. The EMIMCl and EMIMAc were purchased from Haihang Industry Co. Ltd and used as received. The cellulose dissolution in ILs is following a previous report (Stolarska et al., 2017). The EMIMCl and EMIMAc in the weight ratio of 3:7 were accurately weighed, mixed in a Teflon cup, and immersed in an oil bath at 100 °C for 15 minutes. Initially, OPEFB cellulose pulp was added in molten ILs, mixed with

an overhead magnetic stirrer for four hours at 270 rpm for complete dissolution. The dissolved cellulose was analyzed using the Nikon Eclipse microscope under polarized light. The solution is cast on the glass slide and placed on a stage to observe the optimal dissolution time. The cellulosic fiber was regenerated via a dry-jet wet-spinning process. After the cellulose pulp dissolution in ILs was completed, the solution was placed in a stainless steel syringe equipped with a jacket heater (temperature: 100 °C) and extruded into a water bath through a nozzle. The regenerated fibers were stretched using a static roller and collected on the winding roller at the end of the process. The collected regenerated fibers were then soaked overnight in distilled water to remove any residue of ILs and dried at room temperature.

The regenerated cellulose was characterized using Scanning Electron Microscopy (SEM), X-ray diffraction (XRD), Fourier-transform infrared (FTIR) spectroscopy, thermogravimetric analysis (TGA), and tensile testing. Scanning Electron Microscopy (Fei Quanta 450) was used to study the morphology of the RCF. The sample was coated with platinum prior to micrograph recording. Fourier-transform infrared spectroscopy studies of RCF were carried out using Spectrum One (PerkinElmer, USA) spectrometer in the transmission mode (4000-400  $\text{cm}^{-1}$ ) with a resolution of 2  $\text{cm}^{-1}$ . The functional groups of RCF and the presence of ILs are observed. The X-ray diffraction patterns of RCF was obtained with Rigaku MiniFlex II X-ray diffractometer operated at 40 kV and 30 mA using filtered Cu  $K\alpha$  radiation ( $\lambda = 1.5406 \text{ \AA}$ ), and the samples were scanned in the  $2\theta$  range of 5 – 40°. The crystallinity index for RCF was obtained by deconvolution of the XRD pattern. Test of tensile strength for the composites fibers was referred to the ASTM D2256 for the single textile fiber break strength. A Universal testing machine (Tenso Lab) with a 100 N load cell was used to determine the tensile strength, Young's modulus, and elongation at break of the fiber at a constant extension speed of 5 mm/min. The RCF was cut with a length of 250 mm and were then clipped by two clamps in the instrument. The analysis is repeated five times, and the average values of tensile parameters are calculated. Thermogravimetric analysis of untreated and RCF of OPEFB were performed by Mettler Toledo TGA/DSC-1 600 model from 25 to 600 °C under the presence of nitrogen gas atmosphere at a rate of 10 °C  $\text{min}^{-1}$ . The degradation of raw OPEFB cellulose pulp and RCF were analyzed.

## RESULTS AND DISCUSSION

### Solubility of cellulose in a mixture of ILs

To determine the optimum dissolution time, samples were taken at 100 °C at 60 and 120 minutes (Fig. 1). After 60 minutes of OPEFB cellulose dissolution, the fibers formed a water droplet shape indicating that the cellulose had already dissolved in the ILs but was still inhomogeneous. It is suggested that the swelling of polymer solution is the O–H bonding exists in cellulose pulp starts to break and form intramolecular bonding with the anion groups of ILs. The polymer swelling (Fig. 1a) was due to the penetration of solvent resulting in the cellulose structure being unstable, altering the bonding in cellulose while the solid or semi-solid fraction was still undissolved [20]. After 120 minutes, it shows a clear image indicating a transparent and homogeneous OPEFB-IL solution (Fig. 1b). The observed image is similar to previously reported work [2]. It is generally recognized that high temperature and enough time are needed to break multiple inter and intramolecular bonds in cellulose.

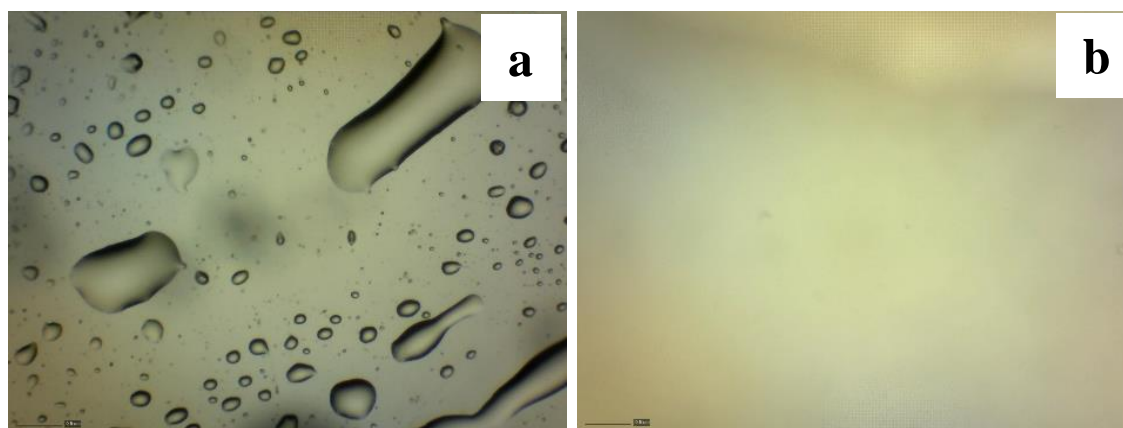


**Figure 1.** Optical microscope images of OPEFB dissolution in ILs mixture after (a) 60 and (b) 120 minutes.

### Mechanism of cellulose dissolution

Cellulose consists of two glucose units linked by glucosidic linkage (C-O-C) at the C1 and C4 positions [14]. The linkage of  $\beta$ -1,4-glycosidic bond in cellulose molecules is responsible for giving cellulose molecules a flat structure making the molecules stack together, forming strong hydrogen bonding. The hydrogen bonding present within individual

sheets and between consecutive sheets makes cellulose strong and insoluble to many organic solvents. The proposed dissolution mechanism of cellulose in a mixture of ILs is illustrated in Fig. 2. The mixture of ILs contains two groups of anions. The chloride ( $\text{Cl}^-$ ) and acetate ( $\text{Ac}^-$ ) anions will form strong O–H bonding with cellulose O–H group, then replacing the hydroxyl groups of cellulose between two cellulosic chains in the equatorial and axial direction [21]. The imidazolium ring cations ( $\text{EMIM}^+$ ) had more interaction with the oxygen and C–H group of cellulose. It was found that the cation will interact through dispersion interaction with the nonpolar group of cellulose while electrostatically interacting with the anion group of cellulose [22]. The mixture of EMIMAc and EMIMCl is an excellent solvent for cellulose and capable of dissolving ~40g of cellulose with 100g of solvent [12]. However, a lower cellulose concentration is practically easier to handle and more cost-efficient [23].

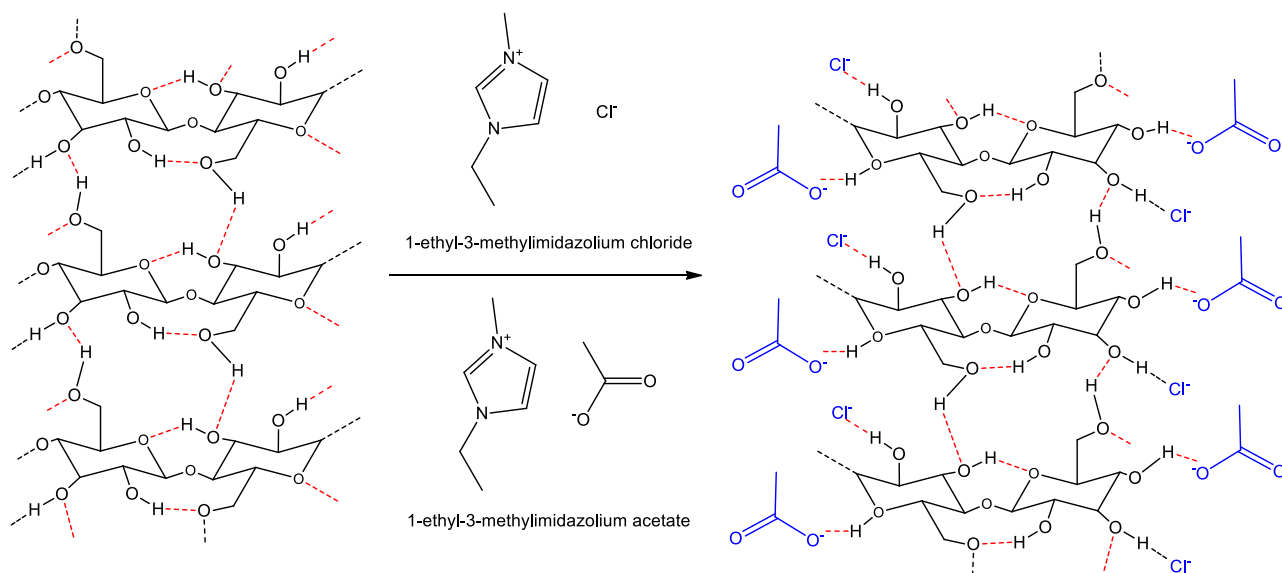


**Figure 2.** Mechanism of OPEFB dissolution.

### Structural analysis of raw OPEFB cellulose pulp and RCF

FTIR analyses were conducted to analyze the structural chemistry of RCF compared with OPEFB cellulose pulp. The obtained IR spectral are shown in Fig. 3 are comparable with several reported literature [3, 12, 24]. The absorption band centered in the  $3600\text{--}3200\text{ cm}^{-1}$  corresponded to the -OH stretching vibration where the RCF shows a stronger peak indicating the chain of molecules in RCF were longer than the OPEFB cellulose pulp [3]. In Fig. 3a, the absorption band at  $2910\text{ cm}^{-1}$  corresponded to C-H stretching vibration, and in comparison, the band shifted to lower wavenumber ( $2899\text{ cm}^{-1}$ ). This indicates that the C-H bond was stretched after cellulose regeneration [12]. The absorption band range at  $1640\text{--}1650\text{ cm}^{-1}$  indicated the O-H bending, which is prominent for RCF due to the absorbed water [25]. The absorption band at  $1389\text{ cm}^{-1}$  shift to lower wavenumber in RCF along with the appearance of new peaks at  $1313, 1261, 1195, 1154, 1027, 897,$  and  $795\text{ cm}^{-1}$ , which can be used for the determination of cellulose I transformed to cellulose II [26]. The peak of  $897\text{ cm}^{-1}$  corresponds to C-O-C stretching vibration  $\beta$ -1,4-glycosidic bonds, which only can be observed at RCF spectra.

The XRD analysis of OPEFB cellulose pulp and RCF are shown in Fig. 4. By using deconvolution method, the characteristic peaks of cellulose and its crystallite size were analyzed and calculated using Scherrer's equation;

$$L = (K \cdot \lambda) / (FWHM \cdot \cos \theta) \quad (1)$$

where,  $L$  is the crystallite size,  $K$  is the Scherrer constant, ( $\approx 0.9$ ),  $\lambda$  is the wavelength of radiation, FWHM is the full width at half maximum of the peak, and  $\theta$  is the peak diffraction angle.

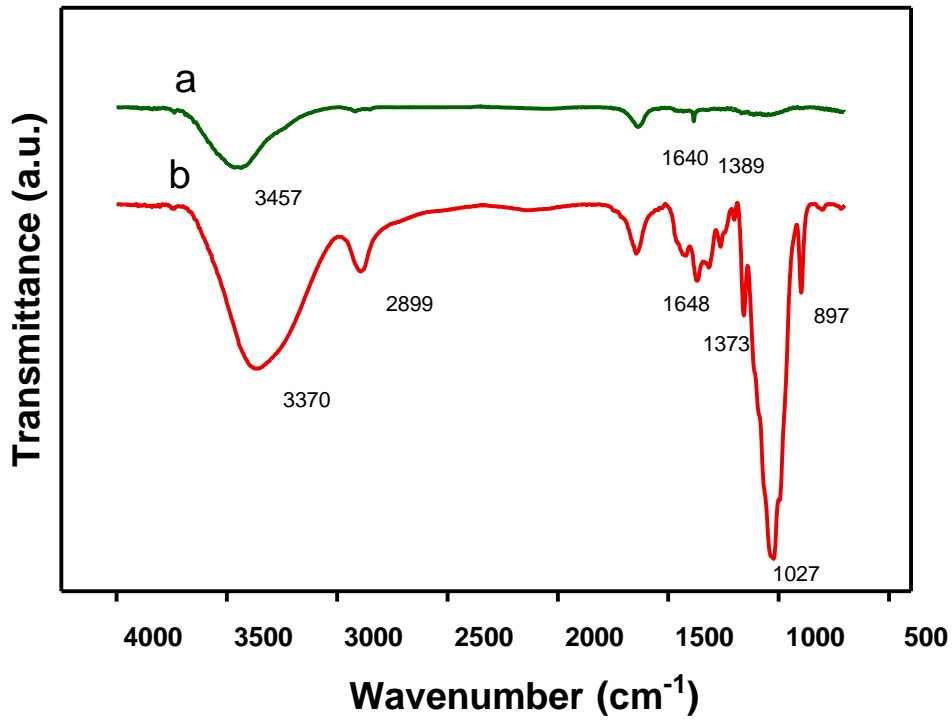


Figure 3. FTIR spectra of (a) raw OPEFB cellulose pulp and (b) RCF.

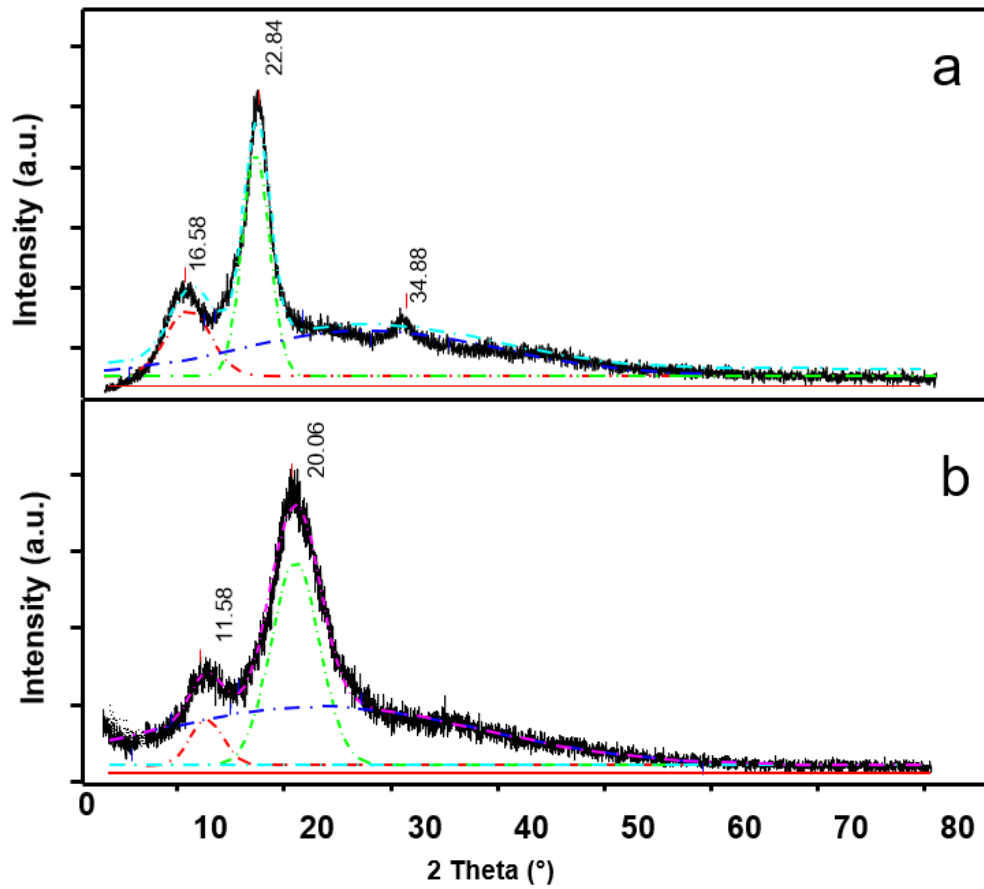


Figure 4. XRD diffraction patterns of (a) raw OPEFB cellulose pulp and (b) RCF.

The XRD data were analyzed using Match! Software and the crystalline lattice of OPEFB cellulose pulp and RCF were monoclinic and similar to previously reported literature [27, 28]. The major difference that can be seen is the highest diffraction peak of raw cellulose pulp at  $2\theta \sim 20.6^\circ$  shift to  $\sim 22.84^\circ$  after regeneration. The stiffer the peak indicates higher crystallinity [28]. Hence, it is demonstrated that the crystallinity decreased after OPEFB cellulose pulp was regenerated. The X-ray patterns of OPEFB (Fig. 4a) is showing diffraction peaks at  $2\theta = 16.8, 22.6,$  and  $34.5^\circ$ , which corresponded to Miller indices of (1 1 0), (2 0 0), and (0 0 4), indicate typical Bragg's angle of Cellulose I [29]. In contrast, diffraction peaks that appear in RCF diffraction, Fig. 4b, at  $2\theta = 12^\circ$  and  $20^\circ$  with crystallographic plane reflections of (-1 1 0) and (1 0 0) were the properties of Cellulose II [28]. The raw OPEFB cellulose pulp was in the crystalline phase and changed to an amorphous phase after regeneration. The crystallinity index of OPEFB cellulose pulp and RCF is 69 and 48%, respectively. It shows that the crystallinity index of OPEFB cellulose pulp significantly decreased after regeneration reaction, due to rearrangement of glycosidic bonds that tends to result in amorphization of RCF. Furthermore, the crystallite size of OPEFB cellulose pulp and RCF is 3.36 and 1.61 nm, respectively. It was noted that the crystallinity index and crystallite size of OPEFB cellulose reduced after regeneration. The possible reason for this behaviour was due to the breaking and reformation of inter and intra-molecular hydrogen bond that exists in cellulose resulting in the decrease in crystallinity index and crystallite size of OPEFB cellulose [30].

### Morphology analysis

The good distribution and arrangement of composition in cellulose filament impacted the mechanical and physical properties of the cellulose filament. The micrograph of longitudinal and cross-section obtained (Fig. 5) is similar to cellulose filament dissolved in 1,5-diazabicyclo[4.3.0]non-5-ene acetate ionic liquid except dissolution in a mixture of EMIMAc and EMIMCl illustrated a round shape cross-sectional structure with rigid and dense structure [31]. The filament also shows a perfectly smooth surface and firm shape (Fig. 5b). It is expected that the good morphological of this filament will oppose satisfying results for other mechanical properties. The diameter of the filament is  $\sim 410$  microns.

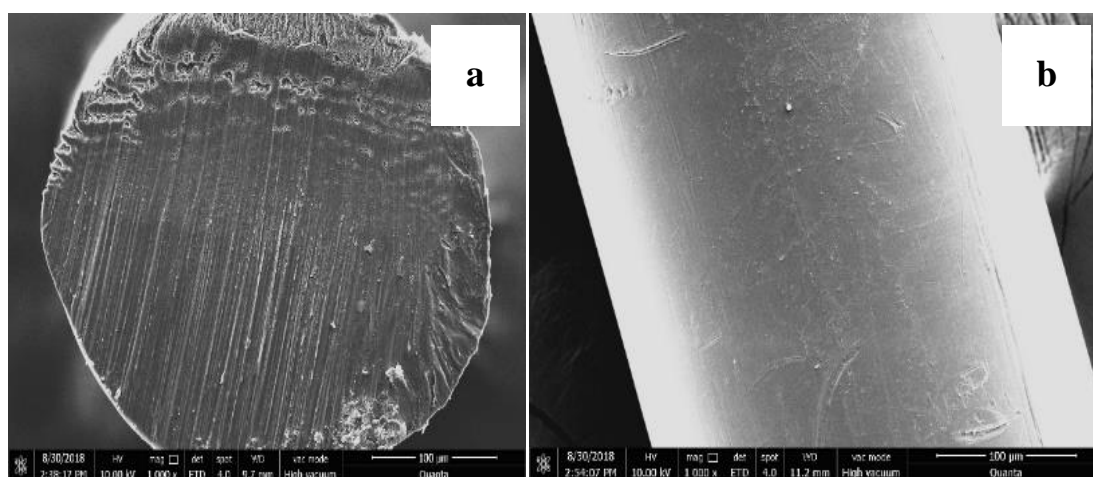


Figure 5. SEM images of (a) the cross-image of RCF filament and (b) longitudinal image of RCF filament.

### Mechanical and thermal properties of raw OPEFB cellulose pulp and RCF

The strain-stress curve of RCF is shown in Fig. 6, and the comparison of tensile strength, Young's modulus, and elongation at break of various RCF were tabulated in Table 1. Tensile strength of RCF was calculated in both mechanical and tenacity units for better comparison with wider applications such as Ioncell-fiber textile. The tensile strength of current studied RCF was compared with [24, 32] that using 8 wt.% of biomass cellulose in IL solvent shows that the current sample resulted in better tensile strength performance. However, this might also be due to the method of regenerating cellulose, as it greatly impacts the mechanical properties of regenerated cellulose. Comparing the value of Young's Modulus and elongation at break, a huge difference can be seen as the results obtained in this study were notably higher values from other studies. Several factors were contributing to the mechanical strength of RCF, including the DP of cellulose, the dissolution temperature, the solvent, relative humidity in the air gap, draw ratio, air gap condition in the water bath (applicable to the dry-jet wet spinning method) and winding speed [17].

TGA analysis was conducted to consider the thermal stability of OPEFB and RCF. The slight initial reduction of weight at temperature  $\sim 100^\circ\text{C}$  was due to the evaporation of adsorbed water content in cellulose [33]. Fig.7 shows that the degradation temperature for both celluloses was similar at  $\sim 271^\circ\text{C}$ . According to [27], the decomposition temperature indicated the thermal stability of the cellulose, which might be attributed to the crystallinity disruption. The obtained

result shows no changes of degradability for both types of cellulose, which can be concluded that even the cellulose was regenerated, the thermal stability remains the same. From Fig. 7a, raw OPEFB cellulose pulp had once decomposition ( $\sim 332^\circ\text{C}$ ), while from Fig. 7b, RCF undergoes double decomposition ( $\sim 295$  and  $\sim 322^\circ\text{C}$ ). This behaviour may be due to crystallinity decrement in RCF (as discussed in structural analysis of XRD) and Cellulose I to Cellulose II transformation. Raw OPEFB cellulose pulp has a wider range of decomposition ( $T_{\text{dec}}$ ) and maximum ( $T_{\text{max}}$ ) decomposition rates, i.e. OPEFB in the range of  $254 - 393^\circ\text{C}$  and RCF in the range of  $234 - 363^\circ\text{C}$ , respectively. The OPEFB cellulose pulp residue was 16 wt%, while RCF was at 25 wt%. The RCF exhibits lower onset temperature but contributes a higher yield of residue during pyrolysis.

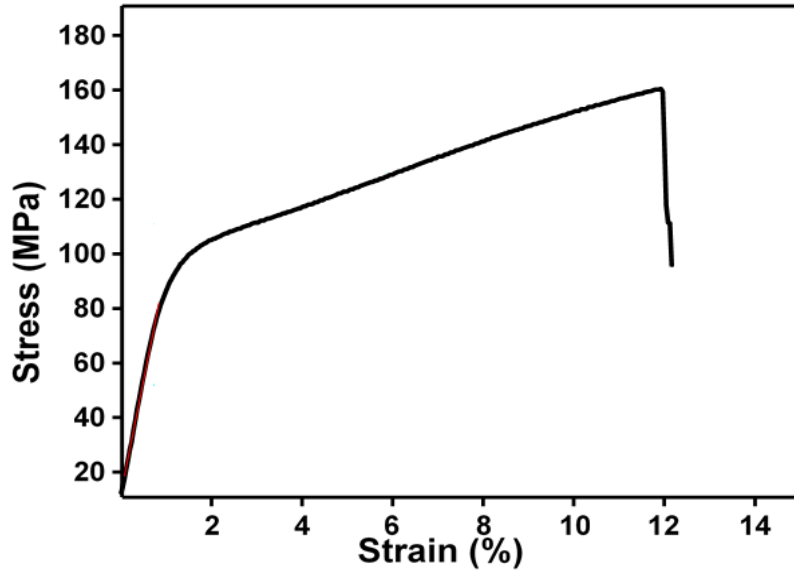


**Figure 6.** Stress-strain curves of RCF.

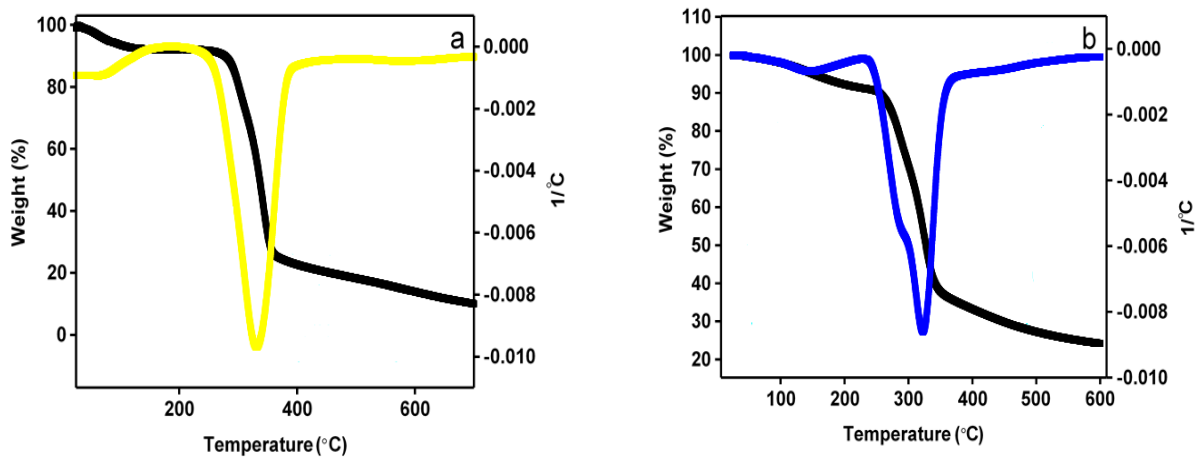


**Figure 7.** Thermogravimetric analysis of (a) raw OPEFB cellulose pulp and (b) RCF.

**Table 1.** The mechanical properties of RCF.

Raw material	Cellulose (%)	Tensile Strength	Young's Modulus (MPa)	Elongation at break (%)	Method of regenerating cellulose	Solvent	Ref.
<b>Eucalyptus urograndis</b>	13	550 (MPa)	23.2	n.a	Dry jet wet spinning	[DBNH] [OAc]	[34]
<b>Eucalyptus urograndis</b>	13	825 (MPa)	20	n.a	Dry jet wet spinning	[DBNH] [OAc]	[35]
<b>Borassus fruit fibers</b>	2	111 (MPa)	6.15	3.1	Casting	AmimCl	[3]
<b>Native wood cellulose pulps</b>	5	0.94 (MPa)	n.a	6.5	Casting	BmimCl	[36]
<b>Oil palm frond</b>	15	11 (MPa)	1.4	n.a	Composite board	BmimCl	[37]
<b>Wood pulp</b>	8	0.293 cN/tex	n.a	7.0	Dry jet wet spinning	BmimCl	[1]
<b>OPEFB</b>	8	71.5±4.4 MPa	n.a	6.6 ± 0.5	Casting	BmimCl	[24]
<b>OPEFB cellulose pulp</b>	8	160.45 ± 0.699 MPa / 8.774 ± 0.699 cN/tex	83.245	12.92 %	Dry-jet wet spinning	EMIMAc + EMIMCl	This study

## CONCLUSION

Cellulose pulp from OPEFB was dissolved in a mixture of EMIMCl and EMIMAc at 100 °C and regenerated with water as anti-solvent by a dry-jet wet spinning method. Even though more cellulose can be dissolved, a small quantity of cellulose was studied as it is easier to handle. From the structural analysis of FTIR and XRD, it is proven that Cellulose I was transformed into cellulose II after regeneration process. The RCF mechanical strength obtained was comparable and had better Young's Modulus and elongation at break properties. Thus, OPEFB cellulose is a promising candidate in sustainable cellulose-based technology applications.

## ACKNOWLEDGEMENT

This work was supported by Universiti Malaysia Pahang Research Grant (RDU1803117) and Postgraduate Research Scheme (PGRS190353).

## REFERENCES

- [1] Cai T, Zhang H, Guo Q, et al (2010) Structure and properties of cellulose fibers from ionic liquids. *Journal of Applied Polymer Science* 115:1047–1053.
- [2] Liu Z, Wang H, Li Z, et al (2011) Characterization of the regenerated cellulose films in ionic liquids and rheological properties of the solutions. *Materials Chemistry and Physics* 128:220–227.
- [3] Reddy KO, Maheswari CU, Dhlamini MS, et al (2017) Preparation and characterization of regenerated cellulose films using borassus fruit fibers and an ionic liquid. *Carbohydrate Polymers* 160:203–211.
- [4] Yuan X, Cheng G (2015) From cellulose fibrils to single chains: understanding cellulose dissolution in ionic liquids. *Phys Chem Chem Phys* 17:31592–31607.
- [5] Faizi MK, Shahriman AB, Abdul Majid MS, et al (2017) An overview of the Oil Palm Empty Fruit Bunch (OPEFB) potential as reinforcing fibre in polymer composite for energy absorption applications. *MATEC Web Conf* 90:01064.
- [6] MPOC: Palm oil production to increase to 19.6 million tonnes in 2021. In: Malaysian Palm Oil Council. <https://mpoc.org.my/mpoc-palm-oil-production-to-increase-to-19-6-million-tonnes-in-2021/>.

- [7] Onoja E, Chandren S, Abdul Razak FI, et al (2019) Oil Palm (*Elaeis guineensis*) Biomass in Malaysia: The Present and Future Prospects. *Waste Biomass Valor* 10:2099–2117.
- [8] Law K-N, Daud WRW, Ghazali A (2007) Morphological and chemical nature of fiber strands of oil palm empty-fruit-bunch (OPEFB). *BioResources* 2:351–362
- [9] Swatloski RP, Spear SK, Holbrey JD, Rogers RD (2002) Dissolution of Cellulose with Ionic Liquids. *J Am Chem Soc* 124:4974–4975.
- [10] Gupta KM, Jiang J (2015) Cellulose dissolution and regeneration in ionic liquids: A computational perspective. *Chemical Engineering Science* 121:180–189.
- [11] Ullah B, Chen J, Zhang Z, et al (2017) 1-Ethyl-3-methylimidazolium acetate as a highly efficient organocatalyst for cyanosilylation of carbonyl compounds with trimethylsilyl cyanide. *Sci Rep* 7:42699.
- [12] Stolarska O, Pawlowska-Zygarowicz A, Soto A, et al (2017) Mixtures of ionic liquids as more efficient media for cellulose dissolution. *Carbohydrate Polymers* 178:277–285.
- [13] Stolarska O, Rodríguez H, Smiglak M (2016) Eutectic mixtures of pyrrolidinium-based ionic liquids. *Fluid Phase Equilibria* 408:1–9.
- [14] Pinkert A, Marsh KN, Pang S, Staiger MP (2009) Ionic Liquids and Their Interaction with Cellulose. *Chem Rev* 109:6712–6728.
- [15] Xia X, Gong M, Wang C, et al (2015) Dynamic modeling of dry-jet wet spinning of cellulose/[BMIM]Cl solution: complete deformation in the air-gap region. *Cellulose* 22:1963–1976.
- [16] Bazbouz MB, Taylor M, Baker D, et al (2019) Dry-jet wet electrospinning of native cellulose microfibers with macroporous structures from ionic liquids. *J Appl Polym Sci* 136:47153.
- [17] Zhang J, Yamagishi N, Tominaga K, Gotoh Y (2017) High-strength regenerated cellulose fibers spun from 1-butyl-3-methylimidazolium chloride solutions. *J Appl Polym Sci* 134:45551.
- [18] Zhu C, Richardson RM, Potter KD, et al (2016) High Modulus Regenerated Cellulose Fibers Spun from a Low Molecular Weight Microcrystalline Cellulose Solution. *ACS Sustainable Chem Eng* 4:4545–4553.
- [19] Chen JY, Sun L, Negulescu II, Xu B (2017) Fabrication and evaluation of regenerated cellulose/nanoparticle fibers from lignocellulosic biomass. *Biomass and Bioenergy* 101:1–8.
- [20] Medronho B, Lindman B (2015) Brief overview on cellulose dissolution/regeneration interactions and mechanisms. *Advances in Colloid and Interface Science* 222:502–508.
- [21] Gross AS, Bell AT, Chu J-W (2011) Thermodynamics of Cellulose Solvation in Water and the Ionic Liquid 1-Butyl-3-Methylimidazolium Chloride. *J Phys Chem B* 115:13433–13440.
- [22] Rabideau BD, Agarwal A, Ismail AE (2014) The Role of the Cation in the Solvation of Cellulose by Imidazolium-Based Ionic Liquids. *J Phys Chem B* 118:1621–1629.
- [23] Kathirgamanathan K, Grigsby WJ, Al-Hakkak J, Edmonds NR (2015) Two-Dimensional FTIR as a Tool to Study the Chemical Interactions within Cellulose-Ionic Liquid Solutions. *International Journal of Polymer Science* 2015:1–9.
- [24] Nor Amalini A, Melina Cheah MY, Wan Rosli WD, et al (2017) Fabrication and characterization of regenerated cellulose films obtained from oil palm empty fruit bunch. *Langkawi, Malaysia*, p 100007
- [25] Mohamed MA, W. Salleh WN, Jaafar J, et al (2016) Regenerated cellulose membrane as bio-template for in-situ growth of visible-light driven C-modified mesoporous titania. *Carbohydrate Polymers* 146:166–173.
- [26] Yu L, Lin J, Tian F, et al (2014) Cellulose nanofibrils generated from jute fibers with tunable polymorphs and crystallinity. *J Mater Chem A* 2:6402.
- [27] Ibrahim F, Moniruzzaman M, Yusup S, Uemura Y (2015) Dissolution of cellulose with ionic liquid in pressurized cell. *Journal of Molecular Liquids* 211:370–372.
- [28] Pang J, Wu M, Zhang Q, et al (2015) Comparison of physical properties of regenerated cellulose films fabricated with different cellulose feedstocks in ionic liquid. *Carbohydrate Polymers* 121:71–78.
- [29] Liu Z, Sun X, Hao M, et al (2015) Preparation and characterization of regenerated cellulose from ionic liquid using different methods. *Carbohydrate Polymers* 117:99–105.
- [30] Zhang J, Wang Y, Zhang L, et al (2014) Understanding changes in cellulose crystalline structure of lignocellulosic biomass during ionic liquid pretreatment by XRD. *Bioresource Technology* 151:402–405.
- [31] Anne Michud, Marjaana Tantu, Shirin Asaadi, et al (2016) Ioncell-F: ionic liquid-based cellulosic textile fibers as an alternative to viscose and Lyocell. *Textile Research Journal* 86:543–552.
- [32] Cai T, Zhang H, Guo Q, et al (2010) Structure and properties of cellulose fibers from ionic liquids. *J Appl Polym Sci* 115:1047–1053.
- [33] Fort DA, Remsing RC, Swatloski RP, et al (2007) Can ionic liquids dissolve wood? Processing and analysis of lignocellulosic materials with 1-n-butyl-3-methylimidazolium chloride. *Green Chem* 9:63–69.
- [34] Hauru LKJ, Hummel M, Michud A, Sixta H (2014) Dry jet-wet spinning of strong cellulose filaments from ionic liquid solution. *Cellulose* 21:4471–4481.
- [35] Michud A, Hummel M, Sixta H (2015) Influence of molar mass distribution on the final properties of fibers regenerated from cellulose dissolved in ionic liquid by dry-jet wet spinning. *Polymer* 75:1–9.
- [36] Peng H, Wang S, Xu H, Dai G (2018) Preparations, properties, and formation mechanism of novel cellulose hydrogel membrane based on ionic liquid. *Journal of Applied Polymer Science* 135.
- [37] Mahmood H, Moniruzzaman M, Yusup S, Akil HMd (2016) Pretreatment of oil palm biomass with ionic liquids: a new approach for fabrication of green composite board. *Journal of Cleaner Production* 126:677–685.